

## Chapter 4

# DETECTORS FOR X-RAY IMAGING AND COMPUTED TOMOGRAPHY

*Advances and Key Technologies*

Michael Overdick

*Philips Research, Aachen, Germany*

**Abstract:** Medical X-ray imaging and Computed Tomography (CT) rely heavily on the performance of the imaging detectors used in these modalities. This article gives an overview over the key technologies involved in the construction of such imaging detectors. Apart from the conversion of the X-rays also photodiodes and the associated electronics constitute important technology fields. For both X-ray and CT the development of the technologies over the last decade is reviewed, the state of the art is described and some current and envisaged developments are emphasized.

**Keywords:** X-ray, CT, detector, scintillator, direct conversion, photodiode, pixel electronics, integrating, counting

## 1. INTRODUCTION

Signal detectors are a central element in any medical imaging system. In the imaging modalities X-ray, CT, SPECT and PET the information is carried by ionizing radiation, more precisely X-rays or  $\gamma$ -quanta. The imaging detectors consist of a multitude of detector channels, for modern X-ray detectors up to several million picture elements (pixels). In this article, the main emphasis will be on detectors for X-ray and CT. SPECT and PET will be briefly touched upon in the outlook section at the end of the article.

In general, detectors for X-ray and CT imaging comprise a conversion stage for converting the X-ray quanta ultimately into electrical signals. The conversion stage is followed by pixel electronics, i.e. the electronic circuitry belonging exclusively to one detector channel. The pixel electronics are then

usually connected to further circuitry, which is shared by many or all detector channels. The general scheme is shown in Figure 4-1a.

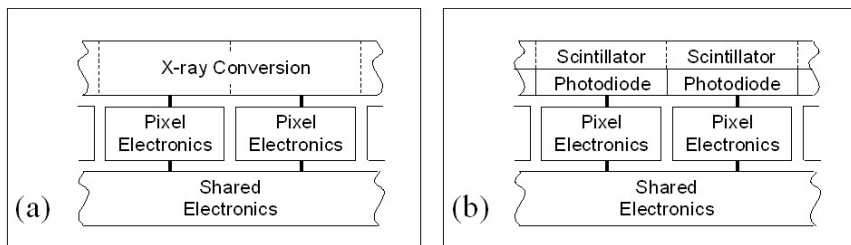


Figure 4-1. a) General representation of an X-ray or CT detector, b) with indirect conversion.

In the majority of today's detectors for dynamic X-ray imaging and CT imaging, the conversion is indirect (Figure 4-1b), i.e. the X-rays are first converted into visible light, which is converted further into an electrical signal by a photosensitive device, usually a photodiode in the case of X-ray and CT. Although the photodiodes are a part of the overall conversion stage, they will be discussed in a separate section of this chapter.

There are many design and performance parameters related to imaging detectors. Detection efficiency, spatial resolution, signal-to-noise ratio, dynamic range and temporal resolution are most important<sup>1</sup>. This article cannot cover all these parameters for all key technologies in depths, so only some main relations will be mentioned.

## 2. CONVERSION MATERIALS

Conversion materials should efficiently detect (i.e. absorb) the incoming X-ray quanta and convert them into light (for scintillating materials) or directly into electrical signals (for direct conversion materials). The extremely strong influence of the conversion stage on the overall imaging performance makes both scintillator and direct conversion materials key technology items for imaging detectors. Main characteristics of conversion materials are:

- Detection efficiency.
- ‘Sensitivity’, i.e. the light yield for scintillators or the charge yield for direct conversion materials.
- Spatial resolution, often expressed as the Modulation Transfer Function (MTF).
- Temporal resolution.

It is very important to note the difference between detection efficiency and sensitivity. As X-ray and CT imaging are governed by the noise of the X-ray quantum flux, the detection efficiency should be as high as possible, e.g. 80% or more of the incoming quanta should be detected. Too low a detection efficiency cannot be recovered by increasing the sensitivity of the detector.

## 2.1 Scintillators

There are many materials emitting visible light when energy is deposited in the material, e.g. by X-rays or energetic charged particles. Such materials are known as scintillators. For the efficient detection of X-rays usually inorganic compounds containing some heavy element are used. Sodium iodide ( $\text{NaI}$ ) or cadmium tungstate ( $\text{CdWO}_4$ ) are well known examples. Extensive overviews have been given by van Eijk<sup>2</sup>. To achieve the high detection efficiency at quantum energies of 60 keV or higher, the typical thickness of a scintillator can range from 0.3 to 2.5 mm for X-ray and CT imaging.

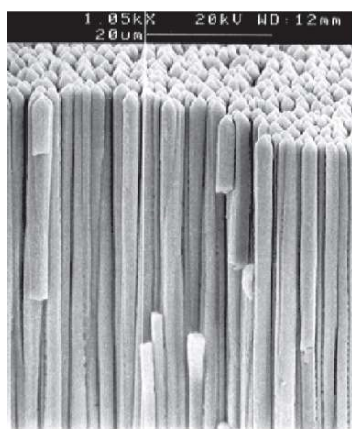


Figure 4-2. Columnar structure of a CsI:Tl scintillator.

X-ray imaging requires a fine spatial resolution of the order of 100  $\mu\text{m}$  at the detector. Cesium iodide ( $\text{CsI}$ ) is often used for this application, as it can be grown with a columnar structure as shown in Figure 4-2. This structure limits the lateral spread of the scintillation light, thus helping significantly in achieving an acceptable spatial resolution. For the use with amorphous silicon photodiodes (see section 3.1), the  $\text{CsI}$  is doped with traces of thallium which works as an activator shifting the maximum of the light emission

spectrum into the green region<sup>3</sup>. The light yield of CsI:Tl is about 60 photons per keV of deposited energy<sup>1,2</sup>. CsI:Tl exhibits a significant afterglow of about 1% after 10 ms<sup>2,4</sup>. However, for X-ray imaging this is an acceptable value. After strong X-ray illumination the light yield of the CsI:Tl increases slightly, the effect being known as ‘bright burn’<sup>4</sup>.

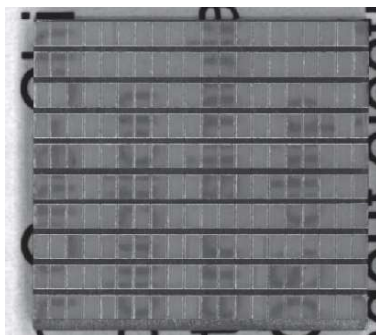


Figure 4-3. Array of CdWO<sub>4</sub> crystals for CT imaging.

For CT imaging the requirements on spatial resolution are only of the order of 1 mm at the detector, while the fast gantry rotation and the large number of projections demand signal integration times as low as 100 µs and therefore a very good temporal behaviour of the scintillator. Frequently cadmium tungstate (CdWO<sub>4</sub>) or gadolinium oxysulfide (GOS, Gd<sub>2</sub>O<sub>2</sub>S) are chosen<sup>5</sup>. CdWO<sub>4</sub> has a light yield of 20 photons per keV, whereas GOS, depending on the doping, reaches 35-60 photons per keV<sup>2</sup>. The scintillator crystals are machined into small pieces of about 2-5 mm<sup>3</sup>, which are then mounted next to each other with reflective material between them to avoid lateral cross-talk of the scintillation light between the individual crystals (Figure 4-3).

## 2.2 Direct conversion materials

Direct conversion materials generate measurable charge signals when absorbing X-ray quanta. Usually these materials have a high resistivity ( $10^{10}$  to  $10^{16}$  Ωcm) and are operated with relatively strong electric fields (between 0.1 and 20 V/µm). For applications in X-ray imaging, several classical photoconducting materials have been studied,<sup>6</sup> such as amorphous selenium<sup>7-9</sup> (a-Se) and the polycrystalline materials lead iodide<sup>10,11</sup> (PbI<sub>2</sub>), lead oxide<sup>12-14</sup> (PbO) and mercury iodide<sup>11,15,16</sup> (HgI<sub>2</sub>). Some properties of these materials are listed in Table 4-1. The main advantage of direct conversion materials is their inherently excellent spatial resolution. Even for

finely spaced pixel electrodes (e.g. 100  $\mu\text{m}$  pitch or below) the charge signal usually remains within the pixel area in which the X-ray quantum was absorbed. This is due to the relatively high and well-defined electric fields in the materials and due to a rather small lateral diffusion of the charge carriers. Figure 4-4 shows an X-ray image obtained with a PbO detection layer<sup>13</sup>. Until now, only amorphous selenium is used in commercial X-ray detectors<sup>7,9</sup>, the other materials still being in their research phases.

*Table 4-1. Selected properties of some direct conversion materials.*

	a-Se	PbO	HgI <sub>2</sub>	cryst. CZT
Typ. el. field	10-20 V/ $\mu\text{m}$	5 V/ $\mu\text{m}$	1-2 V/ $\mu\text{m}$	0.1 V/ $\mu\text{m}$
Resistivity	$10^{14}$ - $10^{16}$ $\Omega\text{cm}$	$10^{12}$ - $10^{13}$ $\Omega\text{cm}$	$10^{12}$ - $10^{13}$ $\Omega\text{cm}$	$3 \cdot 10^{10}$ $\Omega\text{cm}$
Charge yield	20-30 e $^-$ /keV	60 e $^-$ /keV	100 e $^-$ /keV	200 e $^-$ /keV

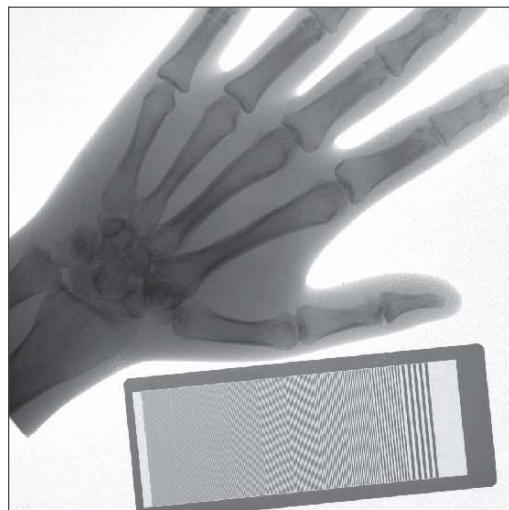


*Figure 4-4. X-ray image acquired with a PbO detection layer.*

A common problem of the amorphous or polycrystalline direct conversion materials is their temporal behavior. Some materials show strong residual signals, i.e. a decaying surplus dark current after X-ray illumination, which can be in the range of several percent still 1 s after switching off the X-rays. Amorphous selenium exhibits a reduced sensitivity (reduced charge yield) after X-ray illumination. This so-called ghosting effect<sup>8</sup> decays even slower, it can be present for minutes. The mechanism of charge trapping cannot account for all of the observed temporal effects in direct converters. Also charge injection invoked by charge accumulation layers may often play a role<sup>14</sup>.

There are also crystalline direct conversion materials. Classical examples are silicon and germanium, but both are not very heavy materials and germanium detectors usually have to be cooled during operation. A room-temperature detector material receiving much research attention is cadmium zinc telluride (CZT, roughly  $\text{Cd}_{0.9}\text{Zn}_{0.1}\text{Te}$ )<sup>17</sup>. Some of its properties are also stated in Table 4-1. CZT has a high charge yield of about 200 e<sup>-</sup> per keV deposited energy, and its temporal behavior is much better than that of amorphous or polycrystalline materials. The use of CZT detector crystals is considered for X-ray, CT and also for SPECT. However, the material is still somewhat expensive and cannot be produced in arbitrary sizes. CZT can also be operated in counting mode allowing the detection of individual X-ray or  $\gamma$ -quanta, as will be discussed in the outlook in section 4.

### **3. PHOTODIODES AND PIXEL ELECTRONICS**

#### **3.1 Flat X-ray detectors based on amorphous silicon**

##### **3.1.1 State of the art**

The field of dynamic X-ray imaging detectors has gone through significant technologies change over the last five years. From the 1970's the standard technology were image intensifier systems (II-TV) based on sizeable vacuum tubes incorporating electron optics, phosphor screens and optical cameras. Roughly from the year 2000 onwards, flat dynamic X-ray detectors<sup>18-21</sup> utilizing amorphous silicon technology have been introduced for cardiology, neurology, vascular imaging and other applications. Also for static X-ray imaging, e.g. in general radiography, the amorphous silicon technology is now frequently employed in new systems.

The majority of the flat X-ray detectors are based on indirect conversion using CsI:Tl as the scintillation material, as discussed in section 2.1. The optical light is detected by amorphous silicon photodiodes in the large area electronics panel<sup>22-24</sup>. The a-Si photodiodes exhibit only small leakage currents and have their maximal sensitivity in the green where the CsI:Tl shows its highest light emission. The circuit diagram for an indirect conversion flat detector pixel is shown in Figure 4-5a. Each pixel has an a-Si thin film transistor (TFT) as the switching element, allowing a row-wise read-out of the pixel array. The pixel diode and its associated capacitance are discharged by the light from the scintillator during X-ray illumination. During read-out an external charge sensitive amplifier (CSA) connected to

the read-out column re-charges the pixel diode to a fixed reverse bias voltage, typically 5 to 10 V. In this charge read-out configuration, the dominant noise sources are the reset noise of the diode (also referred to as kTC-noise as it is given by  $kTC_{pix}$ , where  $C_{pix}$  is the pixel capacitance) and the noise of the charge sensitive amplifier. The shot noise of the diode's leakage current is among the smaller noise contributions.

In addition to the temporal effects in the scintillator, the amorphous silicon photodiode and the TFT in the pixel also show temporal effects<sup>25-28</sup>, namely residual signals, photodiode gain effect (similar to ghosting) and incomplete read-out. The first two effects are attributed to trapping states in the a-Si. Both can be reduced by illuminating the a-Si photodiodes with additional light (refresh light)<sup>28</sup>.

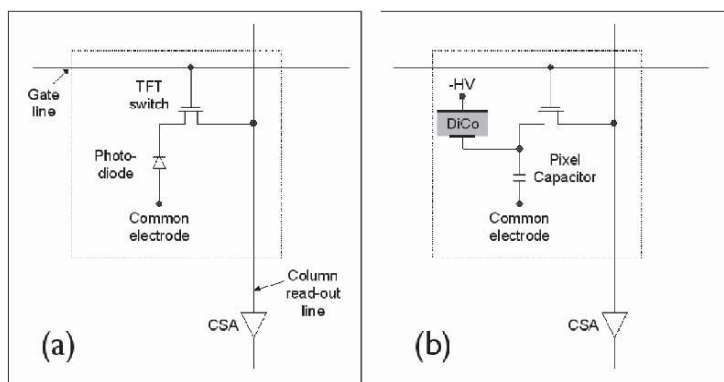


Figure 4-5. a-Si pixel circuits for (a) indirect and (b) direct conversion.

The introduction of flat X-ray detectors based on a-Si technology on the medical market is very successful. Compared to the previous II-TV systems, the flat detectors are less bulky, have a distortion-free imaging geometry and almost completely suppress a long-range blurring effect known as low-frequency drop. For many applications this opens up a larger usable dynamic range.

The flat detectors based on direct conversion materials (see section 2.2) also utilize a-Si technology for the large area substrates<sup>9,13</sup>. The pixel circuit is very similar, as shown in Figure 4-5b. A collection electrode and a capacitor on which the charge signals are integrated during X-ray illumination replace the a-Si photodiode. The read-out operates in a similar way as described for the indirect conversion circuit.

### **3.1.2 Advanced amorphous silicon flat detectors**

After the radical technology switch from image intensifiers to flat X-ray detectors, research and development in this field are currently concentrating on improving the a-Si based X-ray detectors. Improvement topics are the signal-to-noise ratio at low X-ray doses, dynamic range and spatial resolution. Also reducing the production costs and implementing additional functionality within the a-Si technology are natural directions.

One way of improving the signal-to-noise ratio is to enhance the fill factor of the pixel, i.e. the fraction of the pixel area that is sensitive to light. To this end, several methods to increase the size of the photodiode in the pixel have been developed, including diode-on-top technologies<sup>29, 31</sup> and infinite photodiode layers<sup>30</sup>. An increased fill factor also allows to construct detector arrays with smaller pixels and therefore enhanced spatial resolution.

Another way to achieve a higher signal-to-noise ratio would be to amplify the signal already in the pixel. Several circuits for in-pixel amplifiers have been proposed<sup>32-34</sup>. Many suffer from some poor electrical properties of the amorphous silicon TFTs, especially their low charge carrier mobility and the drift of the threshold voltage over time. In more complex circuits also additional noise sources have to be taken into account. An example of a pixel circuit with signal amplification is drawn in Figure 4-6.

Other advanced pixel circuit concepts include the integration of sample-and-hold stages or the suppression of the pixel's reset noise by means of correlated double sampling. Additional functionality can also come in the form of integrated dose sensing allowing the control of the X-ray generation equipment during the X-ray pulse. One concept for integrated dose sensing<sup>35</sup> avoiding any additional active elements in the pixel is shown in Figure 4-7. The dose sensing information is sensed non-destructively through tiny capacitors  $C_{\text{tap}}$  attached to each pixel node. Using appropriate external electronics this yields coarsely resolved images at a very high rate (e.g. 10 kHz) from which the information relevant for the dose control can be derived.

Apart from pure a-Si technology, also advanced technology versions or other large area electronics technologies are investigated. Examples are poly-silicon electronics<sup>34</sup>, or flexible electronics produced by inexpensive roll-to-roll processes, including ink jet printing methods and polymer-based electronics<sup>36</sup>. Also CMOS array detectors have been proposed which can offer excellent performance<sup>37</sup>. However, achieving very large area detectors with sufficient yield may be an issue with this technology.

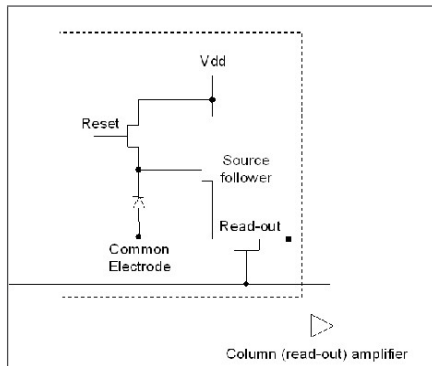


Figure 4-6. Pixel circuit with signal amplification (source follower).

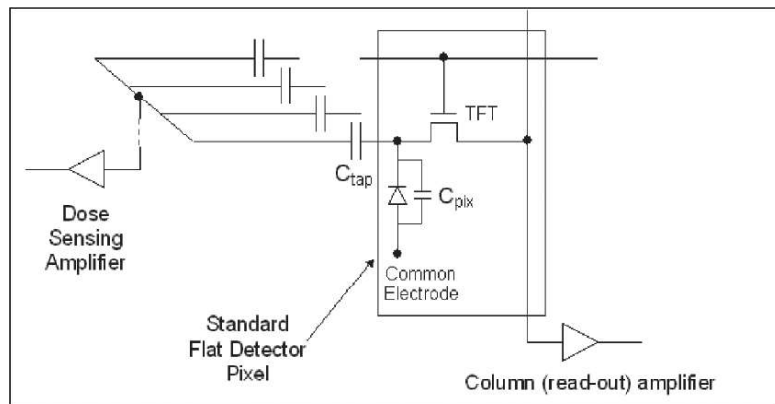


Figure 4-7. Diagram illustrating integrated dose sensing.

### 3.2 Detectors for multi-slice CT

#### 3.2.1 State of the art

In Computed Tomography (CT) the last decade has been dominated by two trends, faster gantry rotation and more detection slices in the axial direction of the patient (multi-slice CT)<sup>38</sup>. Both trends led to a dramatic reduction of the scanning times, shortening a whole body scan, for example, from about 20 minutes to about half a minute. At the same time, the spatial

resolution was improved, leading to even finer resolved volume images of the human body and all organs of interest.

The basic construction scheme of a CT detector has stayed roughly the same. The detector elements are arranged on a ca. 1 m long arc of a circle, sometimes called the ‘detector banana’. Each detector pixel consists of a scintillator crystal and a corresponding photodiode. The photodiode is then connected to the electronics channel, typically comprising an amplifier and an analog-to-digital converter (ADC) optimized for the CT detector operation.

The photodiodes have evolved from individual diodes or linear arrangements into two-dimensional arrays of photodiodes. All of these photodiodes are made from crystalline silicon, which has an excellent linearity and temporal behavior. The illumination is from the front of the photodiode, and the pixel contacts are routed on that same side to one or two edges of the photodiode array. With the number of axial slices in the CT exceeding 32, the routing of the many pixel connections to the edges became more and more difficult. This problem is now addressed using back-illuminated photodiodes, where the routing of the pixel contacts is no longer needed<sup>39,40</sup>. The connection from the pixel is made directly to a substrate using modern interconnect technology.

For the electronics, the increasing number of detector slices led to a strong trend to shrink and integrate the channel electronics, also in order to decrease cost and power consumption and to minimize the noise by keeping the distances between the photodiodes and the electronics short. In current CT detectors, the electronics channels of e.g. 32 pixels fit into an integrated circuit that outputs the digitized data. Also in this context, high density interconnect technologies such as bump bonding are getting more and more important in the field of large area radiation detectors.

### **3.2.2 Advanced technology for CT**

Although today’s CT detectors show an excellent performance, some technologies are being investigated for future CT detectors. One concept brings the integration of the detector one step further by combining the photodiodes and the channel amplifier in a common CMOS chip<sup>41,42</sup>. To achieve the necessary dynamic range of about 17 bit, the amplifier is constructed as an integrator with an automatic gain switch selecting one of two sensitivities. The pixel electronics is located in areas which are in the shadow of the anti-scatter grid of the detector. In this way, the electronics are not wasting valuable fill-factor and are shielded from too much radiation, so that the CMOS pixel electronics is not harmed by the X-rays. Figure 4-8 shows a detector module with 20 by 20 pixels and a zoom into the pixel area.

Other investigations analyze the use of direct conversion materials also for CT. Due to the required excellent temporal behaviour (see section 2.1), the known amorphous and polycrystalline direct conversion materials cannot be used in CT. Only crystalline direct conversion materials are fast enough. Consequently, materials such as cadmium zinc telluride (CZT, see section 2.2) are regarded as possible candidates for use in CT detectors. However, some studies analyzing the behaviour of CZT under high X-ray fluxes indicate some issues with the material<sup>43, 44</sup>.

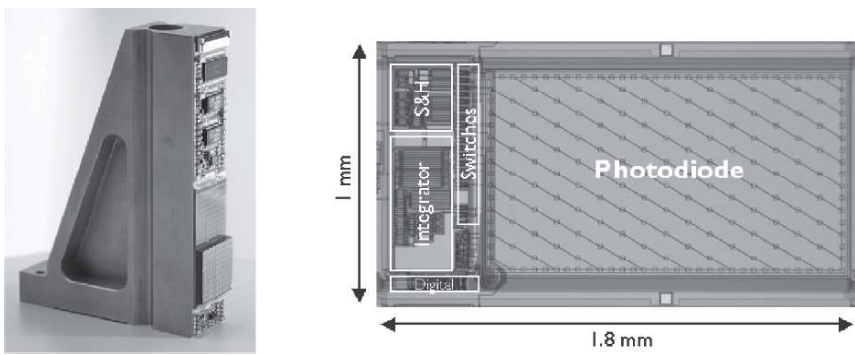


*Figure 4-8.* CT Detector module based on integrated CMOS photodiodes and pixel electronics. On the module, only one of two scintillator arrays is mounted.

#### 4. OUTLOOK

The trends towards higher performance and at the same time cost reduction will continue for detectors in X-ray and CT imaging. In the long run, direct conversion and a further integration of the electronics are probable directions. Apart from this, also qualitative changes in the functionality of the detectors are expected, for example moving from integration mode to counting mode detectors. Until now, both X-ray and CT detectors operate in integration mode, i.e. they sum up the ‘intensity’ of the measured X-ray flux during the signal integration time. An alternative approach is to detect and count the X-ray quanta individually, a mode known as counting operation. Due to the high fluxes that can occur in both X-ray and CT imaging (of the order of  $10^9$  quanta per second per  $\text{mm}^2$  at the detector), counting has so far been considered unfeasible. However, advances in pixellated counting detectors<sup>45, 46</sup> may trigger investigations in this direction.

It is also possible to combine counting and integrating operation, as sketched in Figure 4-9. This would yield additional information as the counting channel records the number of the detected quanta, whereas the integrating channel sums up the energies of the detected quanta. Thus the mean energy of the X-ray quanta can be calculated per detector pixel by simply dividing the integrated signal by the counted signal. The mean energy is a measure for the beam hardening in the patient and can give some information about the material composition along the X-ray beam in the patient. With even more complex electronics it may also become feasible to measure the spectrum of the detected radiation in each pixel<sup>47</sup>. This concept is referred to as spectral X-ray or CT imaging.

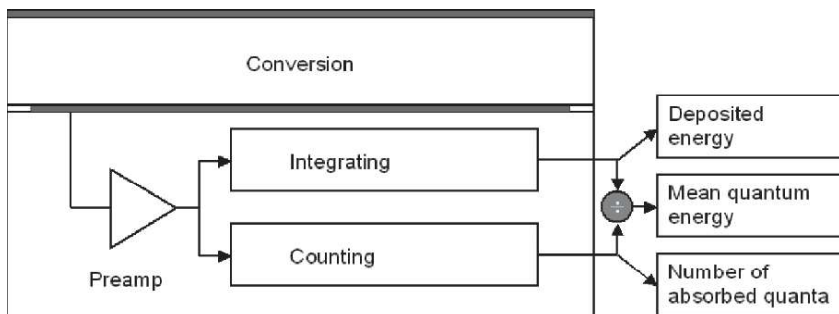


Figure 4-9. Combined counting and integrating detector pixel.

At this point it is interesting to compare the detector technology in X-ray and CT imaging with the methods used in nuclear medicine, i.e. SPECT and PET imaging. In SPECT and PET it is mandatory to measure the energy of the individual  $\gamma$ -quanta to suppress scatter events, so spectral imaging is already a standard in nuclear medicine. However, the fluxes are much lower (1-100 quanta / s mm<sup>2</sup> for SPECT and about 100 quanta / s mm<sup>2</sup> for typical PET applications) which eases the design of the spectrally resolving detector. The architecture still most commonly used in nuclear medicine comprises scintillator crystals optically connected to arrays of photomultipliers. The energy of a detected quantum is calculated by summing up the signals from several adjacent photomultipliers, while the spatial information is retrieved using a centroid calculation. This is the so-called Anger method already in use since the 1960s for two-dimensional scintigraphy. For nuclear medicine a technology change towards solid-state detection with indirect conversion or direct conversion is being contemplated, but most commercial systems still rely on the photomultiplier technology and discrete electronics. More information about the imaging modalities of nuclear medicine can be found in Chapter 8 of this volume.

## 5. CONCLUSIONS

For medical X-ray and CT imaging, the detectors play a significant role for the overall system design and performance. The key technologies comprise:

- X-ray conversion (using scintillators or direct conversion materials).
- Photodiodes (in connection with scintillators).
- Pixel electronics.
- Interconnect technology.

Both X-ray and CT detectors have seen tremendous advances in these key technologies over the last decade. In X-ray imaging the last years brought a rapid technology change from image intensifiers towards flat X-ray detectors based on a-Si large area electronics. This technology is being improved to achieve further enhancements in the detector performance and reductions of the production costs.

For CT detectors, the number of axial slices has increased dramatically and the faster gantry rotation requires shorter and shorter signal integration times. Technically, these challenges have been met by going to back-illuminated photodiodes and highly integrated electronics chips. Also cheap and reliable interconnect technology plays an increasingly important role.

As long-term trends the use of direct conversion materials and even more highly integrated electronics have been identified for both modalities. The future may even bring a qualitative change from integrating detectors to counting detectors also in the field of X-ray and CT imaging.

## ACKNOWLEDGEMENTS

The overview presented here is partly based on the detector related activities at Philips Research Laboratories Aachen, Germany, Philips Research Laboratories Redhill, United Kingdom, Philips Medical Systems X-ray, Best, The Netherlands and Philips Medical Systems CT, Cleveland, Ohio, USA and Haifa, Israel.

The author would like to thank all colleagues from these groups for their contributions and the good long-standing collaboration.

## REFERENCES

1. J. Beutel, H.L. Kundel, R.L. van Metter (eds.), *Handbook of Medical Imaging, Vol. 1*, (SPIE, Bellingham, 2000).
2. C.W.E. van Eijk, Inorganic scintillators in medical imaging, *Phys Med Biol* **47**, R85-R106 (2002).
3. H. Wieczorek et al., CsI:Tl for solid state X-ray detectors, *Proc Int Conf. on Inorganic Scintillators and their Applications (Delft University of Technology)*, 547-554 (1996).
4. H. Wieczorek and M. Overdick, Afterglow and hysteresis in CsI:Tl, *Proc. 5<sup>th</sup> Int Conf on Inorganic Scintillators and their Applications, M.L. Lomonosov Moscow State University*, 385-390 (2000).
5. B.C. Grabmeier, Luminescent materials for medical applications, *J Luminescence* **60&61**, 967-970 (1994).
6. S.O. Kasap and J.A. Rowlands, Direct-conversion flat-panel X-ray image sensors for digital radiography, *Proc IEEE* **90**(4), 591-604 (2002).
7. O. Tousignant et al., Spatial and temporal characteristics of a real-time large area a-Se X-ray detector, *Phys of Med Imaging, Proc SPIE* **5745**, 207-215 (2005).
8. W. Zhao, G. DeCrescenzo, S.O. Kasap, and J.A. Rowlands, Ghosting caused by bulk charge trapping in direct conversion flat-panel detectors using amorphous selenium, *Med Phys* **32**(2), 488-500 (2005).
9. D.C. Hunt, O. Tousignant, J.A. Rowlands, Evaluation of the imaging properties of an a-Se-based flat panel detector for digital fluoroscopy, *Med Phys* **31**(5), 1166-1175 (2004).
10. G. Zentai et al., Improved properties of PbI<sub>2</sub> X-ray imagers with tighter process control and using positive bias voltage, *Phys of Med Imaging, Proc SPIE* **5368**, 668-676 (2004).
11. R.A. Street et al., Comparative study of PbI<sub>2</sub> and HgI<sub>2</sub> for direct detection active matrix X-ray image sensors, *J Appl Phys* **91**(5), 3345-3355 (2002).
12. A. Brauers et al., X-ray sensing properties for a lead oxide photoconductor combined with an amorphous silicon TFT array, *Mat Res Soc Proc* **507**, 321 (1998).
13. M. Simon et al., PbO as direct conversion X-ray detector material, *Phys of Med Imaging, Proc. SPIE* **5368**, 188-199 (2004).
14. M. Simon et al., Analysis of lead oxide (PbO) layers for direct conversion X-ray detectors, accepted for *IEEE Trans Nucl Sc* **52**(5), 2035-2040 (2005).
15. G. Zentai et al., Mercuric iodide medical imagers for low exposure radiography and fluoroscopy, *Phys of Med Imaging, Proc SPIE* **5368**, 200-210 (2004).
16. L.E. Antonuk et al., Systematic development of input-quantum-limited fluoroscopic imagers based on active matrix flat-panel technology, *Phys of Med Imaging, Proc SPIE* **5368**, 127-138 (2004).
17. C. Scheiber and G.C. Giakos, Medical applications of CdTe and CdZnTe detectors, *Nucl Instr Meth A* **458**, 12-25 (2001).
18. N. Jung et al., Dynamic X-ray imaging based on an amorphous silicon thin-film array, *Phys of Med Imaging, Proc SPIE* **3336**, 396-407 (1998).
19. P. R. Granfors, Performance characteristics of an amorphous silicon flat panel X-ray imaging detector, *Phys of Med Imaging, Proc SPIE* **3659**, 480-490 (1999).
20. T. Ducourant et al., Optimization of key building blocks for a large area radiographic and fluoroscopic dynamic digital X-ray detector based on a-Si:H/CsI:Tl flat panel technology, *Phys of Med Imaging, Proc SPIE* **3977**, 14-25 (2000).
21. F. Busse et al., Design and performance of a high-quality cardiac flat detector, *Phys of Med Imaging, Proc SPIE* **4682**, 819-827 (2002).
22. M.J. Powell et al., Amorphous silicon image sensor arrays, *Mat. Res. Soc. Symp. Proc.* **258**, 1127-1137 (1992).

23. R.A. Street et al., Large area 2-dimensional a-Si:H imaging arrays, *Mat Res Soc Symp Proc* **258**, 1145-1150 (1992).
24. L.E. Antonuk et al., Large area, flat-panel a-Si:H arrays for X-ray imaging, *Phys of Med Imaging, Proc SPIE* **1896**, 18-29 (1993).
25. H. Wieczorek, Effects of trapping in a-Si:H diodes, *Solid State Phen* **44-46**, 957-972 (1995).
26. J.H. Siewerdsen and D.A. Jaffray, A ghost story: Spatio-temporal response characteristics of an indirect-detection flat-panel imager, *Med Phys* **26**, 1624-1641 (1999).
27. S. Pourjavid and P.R. Granfors, Compensation for image retention in an amorphous silicon detector, *Phys of Med Imaging, Proc SPIE* **3659**, 501-509 (1999).
28. M. Overdick, T. Solf, H.-A. Wischmann, Temporal artefacts in flat dynamic X-ray detectors, *Phys of Med Imaging, Proc SPIE* **4320**, 47-58 (2001).
29. M.J. Powell et al., Amorphous silicon photodiode thin-film transistor technology with diode on top structure, *Mat Res Soc Symp Proc* **467**, 863-868 (1997).
30. J.T. Rahn et al., High-resolution high fill factor a-Si:H sensor arrays for medical imaging, *Phys of Med Imaging, Proc SPIE* **3659**, 510-517 (1999).
31. R.L. Weisfield et al., Performance analysis of a 127-micron pixel large-area TFT/photodiode array with boosted fill factor, *Phys of Med Imaging, Proc SPIE* **5368**, 338-348 (2004).
32. N. Matsuura, W. Zhao, Z. Huang, J.A. Rowlands, Digital radiology using active matrix readout: Amplified pixel array for fluoroscopy, *Med Phys* **26**(5), 672-681 (1999).
33. K.S. Karim, S. Yin, A. Nathan, J.A. Rowlands, High dynamic range architectures for diagnostic medical imaging, *Phys of Med Imaging, Proc SPIE* **5368**, 657-667 (2004).
34. L.E. Antonuk et al., Investigation of strategies to achieve optimal DQE performance from indirect detection, active matrix flat-panel imagers (AMFPIS) through novel pixel amplification architectures, *Phys of Med Imaging, Proc SPIE* **5745**, 18-31 (2005).
35. M. Overdick et al., Flat detector with integrated dose sensing, *Phys of Med Imaging, Proc SPIE* **5030**, 246-255 (2003).
36. R.A. Street et al., Printed active-matrix TFT arrays for X-ray imaging, *Phys of Med Imaging, Proc SPIE* **5745**, 7-17 (2005).
37. T. Graeve and G.P. Weckler, High-resolution CMOS imaging detector, *Phys of Med Imaging, Proc SPIE* **4320**, 68-76 (2001).
38. J. Hsieh, *Computed Tomography: Principles, Design, Artifacts and Recent Advances*, (SPIE, Bellingham, 2003).
39. R. Luhta et al., Back illuminated photodiodes for multislice CT, *Phys of Med Imaging, Proc SPIE* **5030**, 235-245 (2003).
40. A. Ikhlef et al., Volume CT (VCT) enabled by a novel diode technology, *Phys of Med Imaging, Proc SPIE* **5745**, 1161-1169 (2005).
41. L. Spies et al., Performance of prototype modules of a novel multislice CT detector based on CMOS photosensors, *Phys of Med Imaging, Proc SPIE* **5030**, 490-503 (2003).
42. R. Steadman et al., A CMOS photodiode array with in-pixel data acquisition system for computed tomography, *IEEE J Solid-State Circ* **39**(7), 1034-1043 (2004).
43. A. Jahnke and R. Matz, Signal formation and decay in CdTe X-ray detectors under intense irradiation, *Med Phys* **26**(1), 38-48 (1999).
44. Y. Du et al., Temporal response of CZT detectors under intense irradiation, *IEEE Trans Nucl Sc* **50**(4), 1031-1035 (2003).
45. P. Fischer et al., A counting CdTe pixel detector for hard X-ray and  $\gamma$ -ray imaging, *IEEE Trans Nucl Sc* **48**(6), 2401-2404 (2001).

46. X. Llopart and M. Campbell, First test measurements of a 64k pixel readout chip working in single photon counting mode, *Nucl Inst Meth A* **509**, 157-163 (2003).
47. M. Lindner et al., Medical X-ray imaging with energy windowing, *Nucl Instr Meth A* **465**, 229-234 (2001).